



HAL
open science

Slow Magnetic Relaxation in Chiral Helicene-Based Coordination Complex of Dysprosium

Guglielmo Fernandez-Garcia, Jessica Flores Gonzalez, Jiang-Kun Ou-Yang, Nidal Saleh, Fabrice Pointillart, Olivier Cador, Thierry Guizouarn, Federico Totti, Lahcène Ouahab, Jeanne Crassous, et al.

► **To cite this version:**

Guglielmo Fernandez-Garcia, Jessica Flores Gonzalez, Jiang-Kun Ou-Yang, Nidal Saleh, Fabrice Pointillart, et al.. Slow Magnetic Relaxation in Chiral Helicene-Based Coordination Complex of Dysprosium. *Magnetochemistry*, 2016, 3 (1), 10.3390/magnetochemistry3010002 . hal-01500406

HAL Id: hal-01500406

<https://univ-rennes.hal.science/hal-01500406v1>

Submitted on 14 Dec 2022

HAL is a multi-disciplinary open access archive for the deposit and dissemination of scientific research documents, whether they are published or not. The documents may come from teaching and research institutions in France or abroad, or from public or private research centers.

L'archive ouverte pluridisciplinaire **HAL**, est destinée au dépôt et à la diffusion de documents scientifiques de niveau recherche, publiés ou non, émanant des établissements d'enseignement et de recherche français ou étrangers, des laboratoires publics ou privés.

Slow Magnetic Relaxation in Chiral Helicene-Based Coordination Complex of Dysprosium

Guglielmo Fernandez-Garcia¹, Jessica Flores Gonzalez¹, Jiang-Kun Ou-Yang¹, Nidal Saleh¹, Fabrice Pointillart¹, Olivier Cador¹, Federico Totti², Lahcène Ouahab¹, Jeanne Crassous¹, Boris le Guennic^{1*}

¹ Institut des Sciences Chimiques de Rennes, UMR 6226 CNRS, Université de Rennes 1, 263 Avenue du Général Leclerc 35042 Rennes Cedex;

² Department of Chemistry "Ugo Schiff" and INSTM RU, University of Florence, 50019 Sesto Fiorentino (Italy).

* Correspondence: boris.leguennic@univ-rennes1.fr,

Academic Editor: name

Received: date; Accepted: date; Published: date

Abstract: The complex [Dy(L)(tta)₃] with L the chiral 3-(2-pyridyl)-4-aza[6]-helicene ligand (tta = 2-theonyltrifluoroacetate) has been synthesized in its racemic form and structurally and magnetically characterized. [Dy(L)(tta)₃] behaves as a single molecule magnet in its crystalline phase with the opening of an hysteresis loop at 0.50 K. These magnetic properties were rationalized by *ab initio* calculations.

Keywords: Single molecule magnets; Lanthanide; Helicene; Magnetic anisotropy; *ab initio* calculations

1. Introduction

The design of single molecule magnet (SMM), with the aim of enhance their peculiar magnetic properties, is a prolific field in the scientific community since decades.[1-3] Indeed SMMs can pave the way towards a new generation of materials as, for example, molecular qubits for quantum computing [4], memory storage devices [5] or spin valves [6]. In this framework, lanthanide ions are commonly exploited in the effort of reaching slower relaxation rates for the reversal of the magnetization. Indeed lanthanide are well classified by looking at their electron density distribution, ranging from oblate (planar) to prolate (axial) distribution.[7] This is due mainly to their strong spin-orbit coupling, that leads to ground states with large angular momentum J and to strong magnetic anisotropy. The crystal field, induced by the donor atoms of the ligands, acts only as a perturbation on the electron density distribution, leading to a fine-tuning of the electronic properties and so of the molecular magnetism. As a consequence, the careful choice of the lanthanide ion and of the ligands (and the symmetry) can be used to engineer novel SMMs. However still a complete elucidation of these magneto-structural correlations for these complexes is missing, even if progresses have been done in the past decades.[8-11]

For all the applications mentioned above, it is crucial to study the correlation between the SMM behavior and other physical properties as luminescence or redox activity.[12] The versatility of ligand chemistry can be exploited in this sense to achieve this coupling and may offer the possibility to have in a single compound, for instance, a magnetic emitting nanodevice.[13-15] Indeed, lanthanides have been intensively studied for their peculiar luminescence that covers a broad range of frequency (from visible to NIR) with line-shape emission bands and long lifetime of the excited states.[16-22] However they show very low absorption coefficients, since the f-f transitions are indeed prohibited (Laporte rule).[23] This results in ineffective direct excitation processes, especially in dilute solution. To tackle this problem indirect sensitization, using for example MLCT (Metal-Ligand charge transfer) transitions, has been developed by the mean of functionalization of ligands with organic chromophores acting as antennae.[24] In case the antenna is chiral, the solid-state properties might change between the enantiopure and the racemic crystals. On the other side, the magnetic properties

50 of these atoms can be used to modify the light adsorption in chiral compounds, an effect known as
51 magneto-chiral dichroism.[25-26]

52 A first example of the coupling between a Dy^{III}-based SMM and a chiral antenna has been
53 reported recently with the complex [Dy(L)(hfac)₃] with L = 3-(2-pyridyl)-4-aza[6]-helicene and hfac =
54 1,1,1,5,5,5-hexafluoroacetylacetonate.[27] On the one hand the Dy^{III} ion, with its ⁶H_{15/2} ground state,
55 easily leads to Ising type of magnetic anisotropy in determined coordination spheres like N₂O₆ and
56 this is achieved with the common bidentate 2,2'-bipyridine (bpy) ligand and three hfac ligands.[13,28-
57 30] On the other hand, a 2,2'-bipyridine (bpy) ligand has been functionalized with a [6]-helicene to
58 enhance the luminescence. Indeed, the latter presents a π-conjugated backbone of aromatic rings,
59 configurationally stable for n ≥ 5, and their peculiar topology results in intense emission
60 properties.[31-32] Moreover, [n]-helicene ligands are helically-shaped, so they possess an axial
61 chirality despite the absence of enantiocenter. For all these properties, this family of ligands is widely
62 employed for various applications, ranging from organic molecular electronics,[33] probes for
63 detection of chirality and sensing devices [34] to molecular junction.[35]

64 In the case of the [Dy(L)(hfac)₃] SMM,[27] the chirality of the ligand results in two possible crystal
65 structures (racemic and enantiopure) with similar molecular arrangement but different packings.
66 Interestingly, racemic and enantiopure crystals show notable different magnetic behavior, with the
67 opening of a magnetic hysteresis only in the case of the enantiopure. Moreover, the calculated
68 different nature (anti- and ferromagnetic) of the dipolar couplings between first-neighbors allows
69 explaining the magnetic measurements (e.g. temperature dependence of χ_MT).

70 With the aim to enhance the magnetic properties in this series of compounds, we present herein
71 a novel derivative in which the hfac ligand has been replaced by tta⁻ (2-theonyltrifluoroacetate)
72 ligands. Indeed it is well known in the literature [36-38] that the swapping of these two ligands leads
73 to better magnetic properties. Therefore we report the synthesis, the single crystal X-ray structural
74 analysis and the magnetic characterization along with extensive *ab initio* calculations of the novel
75 compound, [Dy(L)(tta)₃] (**1**).

76

77

78 2. Results and Discussion

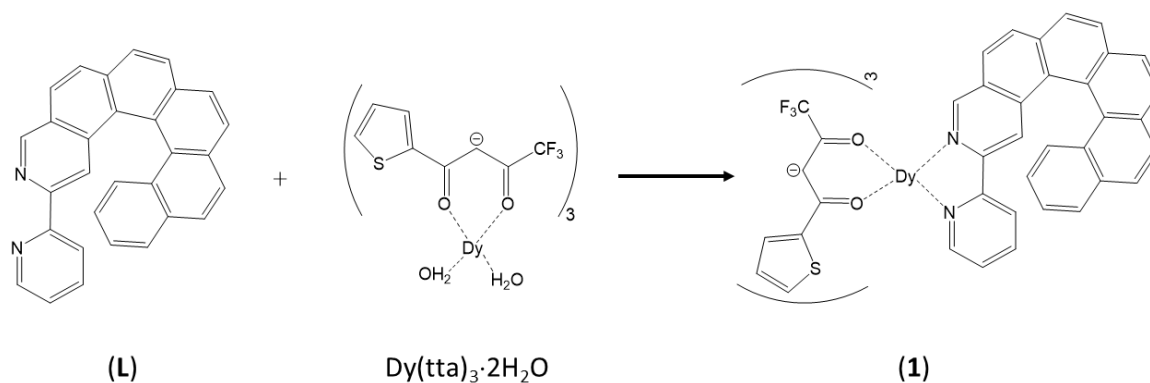
79

80 2.1 Structure

81

82 Complex **1** was obtained by the coordination reaction of the chiral 3-(2-pyridyl)-4-aza[6]-
83 helicene [39] ligand (L) and tris(2-theonyltrifluoroacetate)bis(aqueous)Dy^{III} in CH₂Cl₂ (Scheme 1).

84

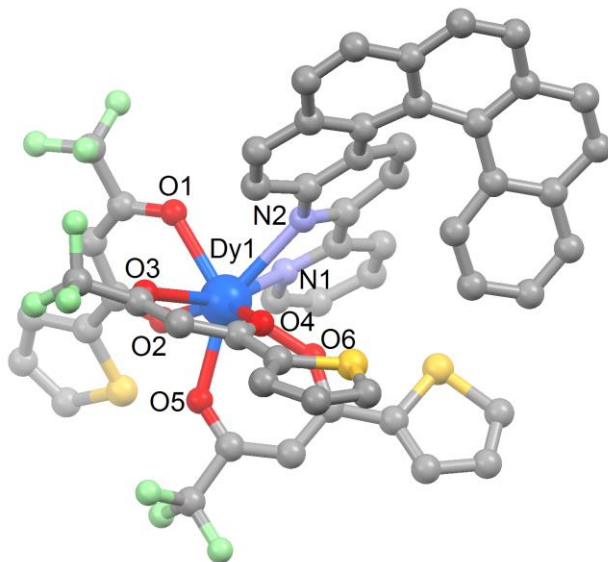


86 **Scheme 1.** Synthetic route to obtain **1**.

87

88 **1** crystallizes in the triclinic centrosymmetric space group P-1 (Figures 1 and S1, Table S1). The
89 Dy^{III} ion is surrounded by two nitrogen atoms and six oxygen atoms coming from the three 2-
90 theonyltrifluoroacetate (tta⁻) anions and the L ligand. The N₂O₆ coordination polyhedron can be
91 described as a distorted square antiprism environment (D_{4d} symmetry, for SHAPE, Table S2).[40]
92 Thus the replacement of the 1,1,1,5,5,5-hexafluoroacetylacetonate anions with tta⁻ one confers an

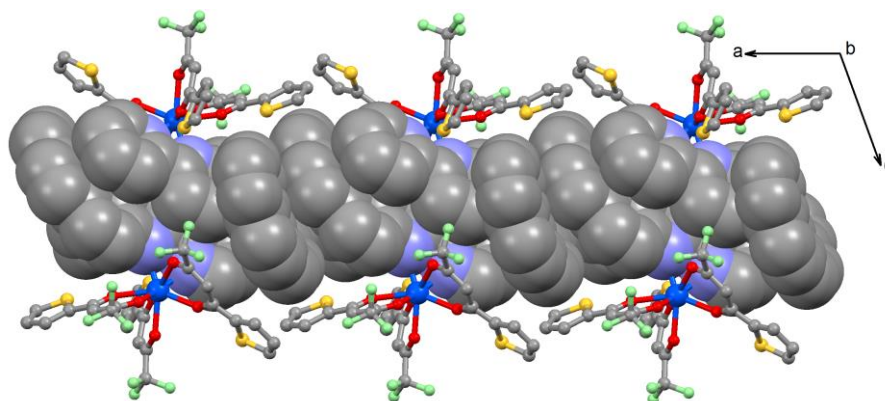
93 higher symmetry for the coordination environment.[27] As already noted, such observation was
94 already done for another complex stemming from group and it has a significant positive impact on
95 the magnetic properties.[37-38]
96
97



98

99 **Figure 1.** (a) Molecular structure of **1**. Hydrogen atoms and molecules of crystallization are omitted for clarity.
100 Selected bond lengths: Dy1-N1, 2.560(3) Å; Dy1-N2, 2.549(3) Å; Dy1-O1, 2.341(3) Å; Dy1-O2, 2.296(3) Å; Dy1-
101 O3, 2.359(3) Å; Dy1-O4, 2.356(3) Å; Dy1-O5, 2.322(3) Å; Dy1-O6, 2.341(3) Å.

102 Starting from the racemic mixture of **L**, both enantiomers are present in the cell. The crystal
103 packing reveals that heterochiral dimers are formed with the presence of π - π interactions between
104 the 2,2'-bipyridyl moieties (Figure 2) while an organic network runs along the *a* axis thanks to π - π
105 interactions between the helicenic parts. The Dy-Dy shortest intermolecular distance was measured
106 equal to 8.935 Å which is similar to the distance measured in the complex involving the Dy(hfac)₃
107 metallo-precursor.
108



109

110 **Figure 2.** Crystal packing of **1** along the *a* axis. “Spacefill” and “ball and sticks” representations are used for **L**
111 ligands and organometallic moieties, respectively.

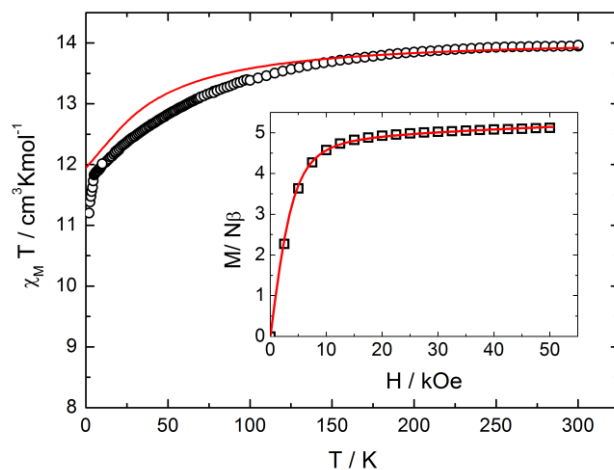
112 2.2 Magnetic properties

113

114 2.2.1 Static magnetic measurements

115

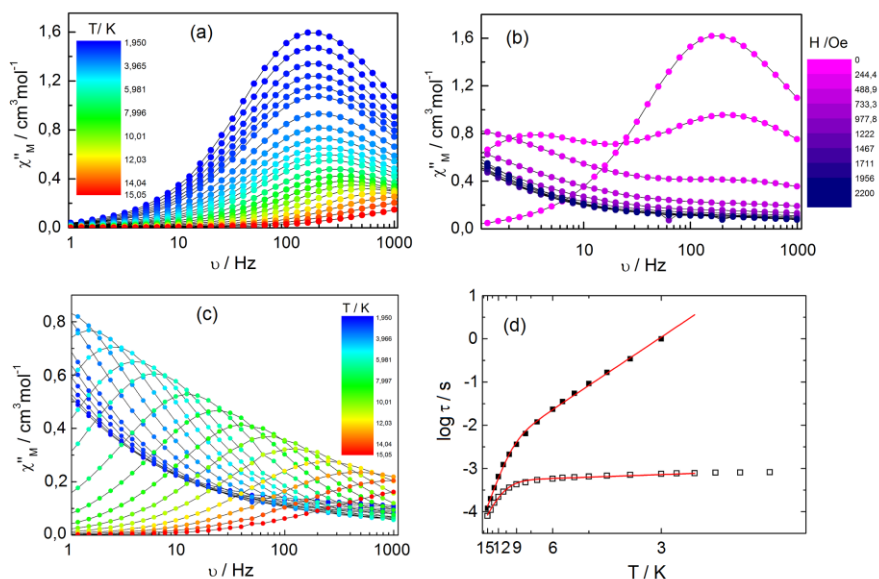
116 The temperature dependence of $\chi_M T$ for the sample **1** is represented in Figure 3. The room
 117 temperature value is $13.96 \text{ cm}^3 \cdot \text{K} \cdot \text{mol}^{-1}$ in good agreement with the expected value of $14.17 \text{ cm}^3 \cdot \text{K} \cdot \text{mol}^{-1}$
 118 ¹ for an isolated Dy^{III} ion.[41] On cooling, $\chi_M T$ decreases monotonically down to $11.20 \text{ cm}^3 \cdot \text{K} \cdot \text{mol}^{-1}$ due
 119 to the thermal depopulation of the M_J states. Below 5K, the more rapid decrease could be attributed
 120 to the presence of weak dipolar antiferromagnetic interactions as determined by quantum
 121 calculations on the analogue complex involving hfac⁻ ancillary ligands.[27] The field dependence of
 122 the magnetization measured at 2.0 K reaches the value of $5.12 \mu_B$ under a magnetic field of 50 kOe,
 123 which is far from the expected saturated value (Inset of Figure 3).
 124



125
 126 **Figure 3.** Temperature dependence of $\chi_M T$ for **1** (black circles). In inset the field variations of the magnetization
 127 at 2 K. Full red lines correspond to the simulated curve from ab initio calculations.

128 2.2.2 Dynamic magnetic measurements

129
 130 The out-of-phase component of the ac susceptibility (χ_M'') of **1** was measured using immobilized
 131 crunched single crystals. It shows frequency dependence in zero external dc field but with clear
 132 maxima of the χ_M'' vs. ν curve (ν the frequency of the ac oscillating field) (Figure 4a). The frequency
 133 dependence of the ac susceptibility can be analyzed in the framework of the extended Debye
 134 model.[42-43] The temperature dependence of the relaxation time at zero field is extracted between
 135 2.0 and 15.0 K (Table S3). The relaxation time follows the Arrhenius law $\tau = \tau_0 \exp(\Delta/kT)$ only above
 136 12 K with $\tau_0 = 7.3(2) \times 10^{-7} \text{ s}$ and $\Delta = 35.4(2) \text{ cm}^{-1}$ (Figure 4d, open squares) while a thermally
 137 independent regime (meanly quantum tunneling of the magnetization, QTM) is observed at lower
 138 temperatures.
 139



140

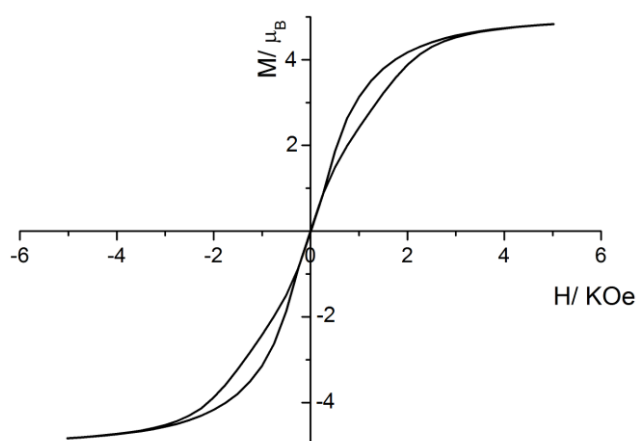
141 **Figure 4.** (a) Frequency dependence of χ''_M between 2 and 15 K, (b) Scan field of the frequency dependence of
 142 χ''_M at 2 K, (c) Frequency dependence of χ''_M between 2 and 15 K under an applied magnetic field of 1000 Oe;
 143 (d) Temperature variation of the relaxation time measured in zero field (open squares) and in an external field
 144 of 1000 Oe (full squares) with the best fitted curve (red lines) in the temperature range of 2-15 K.

145 In order to reduce the QTM operating in this system, the optimal magnetic field of 1000 Oe was
 146 determined by a scan field (Figure 4b). The application of this moderate external dc field induces a
 147 slowing down of the magnetic relaxation with a shift of the maxima of the χ''_M vs. ν curve at lower
 148 frequencies (Figure 4c) Once again the thermal dependence of the relaxation time of the
 149 magnetization can be fitted considering a thermally dependent regime above 10 K (Orbach process)
 150 ($\tau_0 = 2.0(7) \times 10^{-7}$ s and $\Delta = 47.3(3)$ cm $^{-1}$) while at lower temperature the deviation from the linearity can
 151 be attributed to the operating two-phonon Raman process ($\tau = C \times T^n$ with $C = 4.8(6) \times 10^{-3}$ and $n =$
 152 $6.26(7)$).

153 Relaxation times on the order of few seconds is enough slow to observe the opening of the
 154 hysteresis loop at 0.50 K (Figure 5).

155

156



157

158

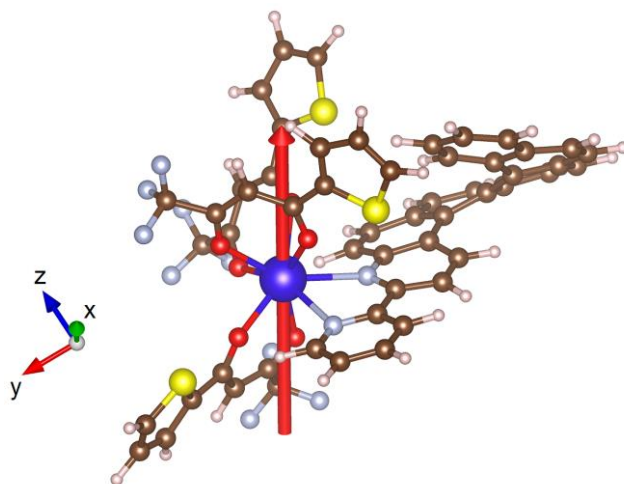
Figure 5. Magnetic hysteresis loop of **1** measured at 0.5 K.

159 2.2.3 Ab initio calculations

160

161 SA-CASSCF/RASSI-SO calculations were performed for **1** to rationalize the observed magnetic
 162 properties (see computational details). The calculated $\chi_M T$ vs T and M vs H (Figure 3) curves fairly

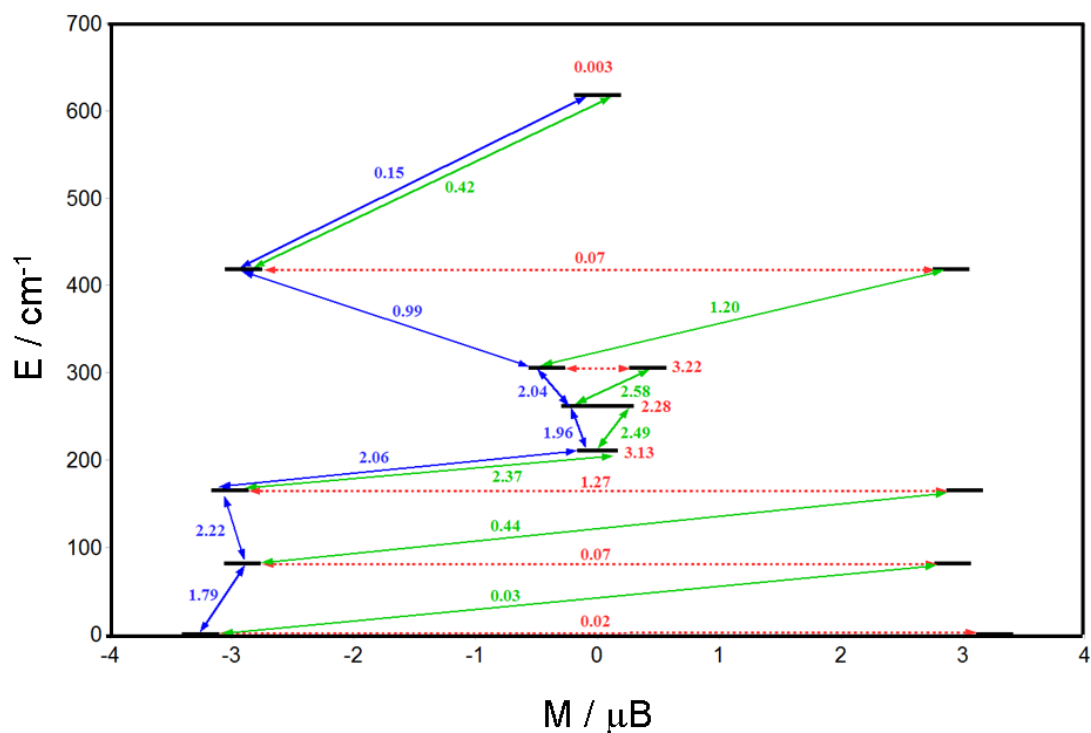
163 well reproduce the experimental curves. Calculations confirm the axial character of the magnetic
164 anisotropy tensor of the ground Kramers doublet with large g_z values of 19.55 and almost negligible
165 g_x and g_y values. The g_z value for Dy^{III} is close to the expected $g_z = 20$ for a pure $M_J = \pm |15/2\rangle$ ground
166 state. This is confirmed by the calculated composition of $M_J = 0.94 |\pm 15/2\rangle + 0.06 |\pm 11/2\rangle$ for the
167 ground doublet state of **1** (see Table S5 for the wavefunction composition). The calculated ground-
168 state easy axis (Figure 6) for the Dy^{III} ion is oriented perpendicular to the plane formed by the 2,2'-
169 bipyridine moieties as expected for an oblate ion in this coordination sphere.[31][36]
170



171
172
173

Figure 6. Representation of complex **1** with the theoretical orientation of the easy magnetic axis of the Dy^{III} center.

174 Moreover, magnetic relaxation pathways can be easily interpreted on the basis of magnetic
175 transition moments (Figure 7) calculated with SINGLE_ANISO program[44-45]. It has to be pointed
176 out that in the latter not all the contribution are included. Indeed the coupling of spin-phonon degrees
177 of freedom in the SMM relaxation is not taken into account in the *ab initio* model whereas it has been
178 recently evidenced its general importance.[46-47] However these discrepancies are common in
179 literature [3][48-49] and the magnetic transition moments calculated in this work still leads to a fairly
180 good qualitative picture. Indeed no direct transition between the two M_J states of the ground doublet
181 or Orbach processes from the ground state are expected whereas relaxation mechanisms involving
182 states from the third M_J state are highly probable. A non-negligible Orbach process has been found
183 also between the second and third M_J states. The calculations indicate a difference between the
184 calculated energy barrier ($\Delta = 82 \text{ cm}^{-1}$) and the experimental barrier ($\Delta = 35\text{-}47 \text{ cm}^{-1}$). However the
185 discrepancy between these values has to be ascribed in the spin-phonon contributions mentioned
186 above.
187



188

189 **Figure 7.** Computed magnetization blocking barrier in complex **1** for the Dy^{III} ion. Numbers provided on each
 190 arrow are the mean absolute values for the corresponding matrix elements of the magnetic transition dipole
 191 moment.

192

193

194 3. Conclusions

195

196 In the course of intermixing chirality offered by the nature of the ligands and SMM properties,
 197 we extend herein the family of [6]-helicene-based lanthanide SMM.[27] We report the synthesis of
 198 the complex [Dy(L)(tta)₃] with **L** the chiral 3-(2-pyridyl)-4-aza[6]-helicene ligand (tta⁻ = 2-
 199 theonyltrifluoroacetate). Its racemic form was structurally and magnetically characterized.
 200 [Dy(L)(tta)₃] behaves as a single molecule magnet in its crystalline phase. As expected, the
 201 substitution of hfac⁻ ligands by tta⁻ moieties enhances the magnetic behavior with the opening of an
 202 hysteresis loop at 0.50 K that was only observed for the enantiopure forms in the case of
 203 [Dy(L)(hfac)₃].[27] In the near future, we will pursue our investigation of chiral lanthanide-based
 204 SMMs that may offer new perspectives in both the domains of molecular magnetism and chirality
 205 with the potential access of properties such as circularly polarized luminescence (CPL) activity that
 206 remains anecdotic for lanthanide compounds to date.

207 Materials and Methods

208 1. Synthesis. General Procedures and Materials

209 The precursor Dy(tta)₃·2H₂O [50] (tta⁻ = 2-theonyltrifluoroacetate anion) and the ligand 3-(2-
 210 pyridyl)-4-aza[6]-helicene [39, 51] **L** were synthesized following previously reported methods. All
 211 other reagents were commercially available and used without further purification.

212 2. Synthesis of complex [Dy(tta)₃(L)]·CH₂Cl₂·C₇H₈ (**1**)

213 Dy(tta)₃·2H₂O (17.2 mg, 0.02 mmol) were dissolved in 5 mL of CH₂Cl₂ and then added to a
 214 solution of 5 mL of CH₂Cl₂ containing 8.3 mg of **L** (0.02 mmol). After 20 minutes of stirring, 30 mL of
 215 toluene were layered at 4°C in the dark. Slow diffusion following by slow evaporation lead to yellow

216 single crystals which are suitable for X-ray studies. Yield: 15.2 mg (54 % based on Dy). Anal. Calcd
217 (%) for $C_{62}H_{40}Cl_2DyF_9N_2O_6S_3$: C 52.78, H 2.84, N 1.99; found: C 52.72, H 2.81, N, 2.09. I.R. 3426 (m),
218 2923 (w), 1604 (s), 1588 (m), 1566 (m), 1493 (m), 1468 (m), 1429 (m), 1256 (s), 117 (m), 1091 (w), 1046
219 (w), 991 (w), 963 (w), 848 (w), 815 (w), 797 (s), 773 (m), 755 (m), 654 (m), 542 (m), 503 (m) cm^{-1} .

220 3. Crystallography

221 Single crystal of $[Dy(tta)_3(L)] \cdot CH_2Cl_2 \cdot C_7H_8$ (**1**) was mounted on a APEXII Bruker-AXS
222 diffractometer for data collection (MoK α radiation source, $\lambda = 0.71073 \text{ \AA}$). The structure was solved
223 by direct methods using the SIR-97 program and refined with a full matrix least-squares method on
224 F^2 using the SHELXL-97 program [1]. Crystallographic data are summarized in Table S1. Complete
225 crystal structure results as a CIF file including bond lengths, angles, and atomic coordinates are
226 deposited as Supporting Information. CCDC number is 1510324 for compound **1**.

227 4. Physical Measurements

228 The elementary analyses of the compound were performed at the Centre Régional de Mesures
229 Physiques de l'Ouest, Rennes. The dc magnetic susceptibility measurements were performed on solid
230 polycrystalline sample with a Quantum Design MPMS-XL SQUID magnetometer between 2 and 300
231 K in an applied magnetic field of 0.2 T for temperatures in the range 2-20 K and 1 T for temperatures
232 between 20 and 300 K. These measurements were all corrected for the diamagnetic contribution as
233 calculated with Pascal's constants.

234 5. Computational Details

235 Wavefunction-based calculations were carried out on molecular structures of **1** by using the SA-
236 CASSCF/RASSI-SO approach, as implemented in the MOLCAS quantum chemistry package
237 (versions 8.0).[52] In this approach, the relativistic effects are treated in two steps on the basis of the
238 Douglas–Kroll Hamiltonian. First, the scalar terms were included in the basis-set generation and were
239 used to determine the spin-free wavefunctions and energies in the complete active space self-
240 consistent field (CASSCF) method.[53] Next, spin-orbit coupling was added within the restricted-
241 active-space-state-interaction (RASSI-SO) method, which uses the spin-free wavefunctions as basis
242 states.[54-55] The resulting wavefunctions and energies are used to compute the magnetic properties
243 and g-tensors of the lowest states from the energy spectrum by using the pseudo-spin $S = 1/2$
244 formalism in the SINGLE-ANISO routine [44-45]. Cholesky decomposition of the bielectronic
245 integrals was employed to save disk space and speed-up the calculations. [56] For **1** the active space
246 of the self consistent field (CASSCF) method consisted of the nine 4f electrons of the Dy^{III} ion spanning
247 the seven 4f orbitals, i.e. CAS(9,7)SCF. State-averaged CASSCF calculations were performed for all of
248 the sextets (21 roots), all of the quadruplets (224 roots), and 300 out of the 490 doublets (due to
249 software limitations) of the Dy^{III} ion. Twenty-one sextets, 128 quadruplets, and 107 doublets were
250 mixed through spin-orbit coupling in RASSI-SO. All atoms were described by ANO-RCC basis sets.
251 [57-59] The following contractions were used: [8s7p4d3f2g1h] for Dy, [4s3p2d1f] for the O and N
252 atoms, [3s2p1d] for the C and F atoms, [4s3p1d] for the S atoms and [2s1p] for the H atoms. The atomic
253 positions were extracted from the X-ray crystal structures. Only the position of the H and F atoms
254 were optimized on the Y^{III} parent complexes with the Gaussian 09 (revision D.01) package [60]
255 employing the PBE0 hybrid functional. [61] The “Stuttgart/Dresden” basis sets [62] and effective core
256 potentials were used to describe the yttrium atom, whereas all other atoms were described with the
257 SVP basis sets [63].

258 **Supplementary Materials:** The following are available online at www.mdpi.com/link, Figure S1: ORTEP view
259 of **1**. Thermal ellipsoids are drawn at 30% probability. Hydrogen atoms and solvent molecules of crystallization
260 are omitted for clarity., Figure S2: Frequency dependence of the ac susceptibility components χ_M' and χ_M'' at 10
261 K and in zero external dc field for compound **1** with the best fitted curve with extended Debye model, Figure S3:
262 Frequency dependence of the ac susceptibility components χ_M' and χ_M'' at 10 K and in 1000 Oe external dc field
263 for compound **1** with the best fitted curve with extended Debye model; Figure S4: Cole-Cole plots using the ac

264 data performed under zero magnetic field. The black lines correspond to the fit with a generalized Debye model;
265 Figure S5: Cole-Cole plots using the ac data performed under 1000 Oe magnetic field. The black lines correspond
266 to the fit with a generalized Debye model; Figure S6: Magnetic hysteresis loop of **1** measured at 0.5, 1.0 and 1.5
267 K; Table S1: X-ray crystallographic data of **1**; Table S2: SHAPE analysis for **1**; Table S3: Best fitted parameters (χ_T ,
268 χ_S , τ and α) with the extended Debye model **1** at zero field in the temperature range 2.0-15 K; Table S4: Best
269 fitted parameters (χ_T , χ_S , τ and α) with the extended Debye model **1** at 1kOe in the temperature range 1.8-5 K;
270 Table S5: Computed energies, g -tensor and wavefunction composition of the ground state doublet in the effective
271 spin $\frac{1}{2}$ model for **1**.

272 **Acknowledgments:** This work was supported by Région Bretagne, Rennes Métropole, CNRS, Université de
273 Rennes 1. G.F.G gratefully acknowledges the European Commission through the ERC-AdG 267746
274 MolNanoMas (project n. 267746) and the ANR (ANR-13-BS07-0022-01) for financial support. N.S. and J.-K.O.-Y.
275 respectively thank the ANR (ANR-10-BLAN-724-1-NCPCHEM) and the Chinese Scholarship Council for
276 financial support. B.L.G. and G.F.G. thank the French GENCI/IDRIS-CINES center for high-performance
277 computing resources.

278 **Author Contributions:** J.-K. O. and N. S. performed the organic syntheses; F. P. performed the coordination
279 chemistry, crystallizations, the single crystal X-ray diffraction experiments and structure refinements; O.C.
280 performed the magnetic measurements, J. F. G. analyzed the magnetic measurements. G. F.-G., F. T. and B. L. G.
281 performed the ab initio calculations. J. C. and L. O. discussed the results and commented on the manuscript.
282 F.P., O.C. and B.L.G. conceived and designed the experiments and contributed equally to the writing of the
283 article.

284 **Conflicts of Interest:** The authors declare no conflict of interest. The founding sponsors had no role in the design
285 of the study; in the collection, analyses, or interpretation of data; in the writing of the manuscript, and in the
286 decision to publish the results.

287 Abbreviations

288 The following abbreviations are used in this manuscript:

289 SMM: Single Molecule Magnet
290 TTF: TetraThiaFulvalene
291 CH_2Cl_2 : Dichloromethane
292 hfac: 1,1,1,5,5,5-hexafluoroacetylacetonate
293 tta: 2-theonyltrifluoroacetate
294 PCM: Polarizable Continuum Model
295 CASSCF: Complete Active Space Self-Consistent Field
296 RASSI-SO: Restricted Active Space State Interaction – Spin-Orbit

297 References

298 © 2016 by the authors; licensee MDPI, Basel, Switzerland. This article is an open access article distributed under
299 the terms and conditions of the Creative Commons by Attribution (CC-BY) license
300 (<http://creativecommons.org/licenses/by/4.0/>).

- [1] Sessoli, R.; Powell, A. K. Strategies towards single molecule magnets based on lanthanide ions. *Coord. Chem. Rev.* **2009**, *253*, 2328-2341.
- [2] Liddle, S.; Slageren, J. Improving f-element single molecule magnets. *Chem. Soc. Rev.*, **2015**, *44*, 6655-6669.
- [3] Pedersen, K. S.; Dreiser, J.; Weihe, H.; Sibille, R.; Johannesen, H. V.; Sorensen, M. A.; Nielsen, B. E.; Sigrist, M.; Mutka, H.; Rols, S.; Bendix, J.; Piligkos, S. Design of Single-Molecule Magnets: Insufficiency of the Anisotropy Barrier as the Sole Criterion. *Inorg. Chem.*, **2015**, *54*, 7600-7606.
- [4] Pedersen, K. S.; Ariciu, A.; McAdams, S.; Weihe, H.; Bendix, J.; Tuna, F.; Piligkos, S. Toward Molecular 4f Single-Ion Magnet Qubits. *J. Am. Chem. Soc.*, **2016**, *138*, 5801-5804.
- [5] Mannini, M.; Pineider, F.; Sainctavit, P.; Danieli, C.; Otero, E.; Sciancalepore, C.; Talarico, A. M.; Arrio, M.-A.; Cornia, A.; Gatteschi, D. Magnetic memory of a single-molecule quantum magnet wired to a gold surface. *Nat. Mater.* **2009**, *8*, 194-197.
- [6] Rocha, A. R.; García-Suárez, V. M.; Bailey, S. W.; Lambert, C. J.; Ferrer, J.; Sanvito, S. Towards Molecular Spintronics. *Nat. Mater.* **2005**, *4*, 335-339.

- [7] Rinehart, J. D.; Long, J. R. Exploiting single-ion anisotropy in the design of f-element single-molecule magnets. *Chem. Sci.* **2011**, *2*, 2078-2085.
- [8] Lucaccini, E.; Briganti, M.; Perfetti, M.; Vendier, L.; Costes, J.-P.; Totti, F.; Sessoli, R.; Sorace, L. Relaxation Dynamics and Magnetic Anisotropy in a Low-Symmetry Dy^{III} Complex. *Chem. Eur. J.*, **2016**, *22*, 5552-5562.
- [9] Zhang, P.; Zhang, L.; Tang, J. Lanthanide single molecule magnets : progress and perspective. *Dalton. Trans.* **2015**, *44*, 3923-3929.
- [10] Zhang, P.; Jung, J.; Zhang, L.; Tang, J.; Le Guennic, B. Elucidating the Magnetic Anisotropy and Relaxation Dynamics of Low-Coordinate Lanthanide Compounds. *Inorg. Chem.* **2016**, *55*, 1905-1911.
- [11] Cucinotta, G.; Perfetti, M.; Luzon, J.; Etienne, M.; Car, P. E.; Caneschi, A.; Calvez, G.; Bernot, K.; Sessoli, R. Magnetic Anisotropy in a Dysprosium/DOTA Single-Molecule Magnet : Beyond Simple Magneto-Structural Correlations. *Angew. Chem., Int. Ed.*, **2012**, *51*, 1606-1610.
- [12] Pointillart, F.; Le Guennic, B.; Cador, O.; Maury, O.; Ouahab, L. Lanthanide and Ion and Tetrathiafulvalene-Based Ligand as a "Magic" Couple toward Luminescence, Single Molecule Magnets, and Magnetostructural Correlations. *Acc. Chem. Res.* **2015**, *48*, 2834-2842.
- [13] Pointillart, F.; Jung, J.; Berraud-Pache, R.; Le Guennic, B.; Dorcet, V.; Golhen, S.; Cador, O.; Maury, O.; Guyot, Y.; Decurtins, S.; Liu, S.; Ouahab, L. Luminescence and Single-Molecule Magnet Behavior in Lanthanide Complexes Involving a Tetrathiafulvalene-Fused Dipyrrophenazine Ligand. *Inorg. Chem.*, **2015**, *54*, 5384-5397.
- [14] Long, J.; Vallat, R.; Ferreira, R. A. S.; Carlos, L. D.; Almeida Paz, F. A.; Guari, Y.; Larionova, J. A bifunctional luminescent single-ion magnet: towards correction between luminescence studies and magnetic slow relaxation processes. *Chem. Commun.*, **2012**, *48*, 9974.
- [15] Pointillart, F.; Le Guennic, B.; Golhen, S.; Cador, O.; Maury, O.; Ouahab, L. A redox active luminescent ytterbium single-molecule magnet. *Chem. Commun.*, **2013**, *49*, 615-617.
- [16] Sabbatini, N.; Guardigli, M.; Manet, I. Handbook of the Physics and Chemistry of Rare Earths, Vol. 23, Elsevier, Amsterdam, 1996, p. 69.
- [17] Comby, S.; Bünzli, J.-C. G. Handbook on the Physics and Chemistry of Rare Earths, Vol. 37, Elsevier, Amsterdam, 2007; Chapter 235.
- [18] Parker, D. Luminescent Lanthanide Sensors for pH, pO₂ and Selected Anions. *Coord. Chem. Rev.* **2000**, *205*, 109-130.
- [19] Parker, D. Excitement in f block: structure, dynamics and function of nine-coordinate chiral lanthanide complexes in aqueous media. *Chem. Soc. Rev.* **2004**, *33*, 156-165.
- [20] Bünzli, J.-C. G.; Piguet, C. Taking advantage of luminescent lanthanide ions. *Chem. Soc. Rev.* **2005**, *34*, 1048-1077.
- [21] S. V. Eliseeva, J.-C. G. Bünzli, Lanthanide luminescence for functional materials and bio-sciences. *Chem. Soc. Rev.* **2010**, *39*, 189-227.
- [22] D'Aléo, A.; Pointillart, F.; Ouahab, L.; Andraud, C.; Maury, O. Charge transfer excited states sensitization of lanthanide emitting from the visible to the near-infra-red. *Coord. Chem. Rev.* **2012**, *256*, 1604-1620.
- [23] VanVleck, J. H. The Puzzle of rare-earth Spectra in Solids. *J. Phys. Chem.* **1937**, *41*, 67-80.
- [24] Wang, X.; Chang, H.; Xie, J.; Zhao, B.; Liu, B.; Xu, S.; Pei, W.; Ren, N.; Huang, L.; Huang, W. Recent developments in Lanthanide-based luminescent probes. *Coord. Chem. Rev.* **2014**, *273-274*, 201-212.
- [25] Train, C.; Ghoerghe, R.; Krstic, V.; Chamoreau, L.; Ovanesyan, N. S.; Rikken, G. L. J. A.; Gruselle, M.; Verdaguer, M. Strong magneto-chiral dichroism in enantiopure chiral ferromagnets. *Nat. Mater.*, **2008**, *7*, 729-734.
- [26] Sessoli, R.; Boulon, M.-E.; Caneschi, A.; Mannini, M.; Poggini, L.; Wilhelm, F.; Rogalev, A. Strong magneto-chiral dichroism in a paramagnetic molecular helix observed by hard X-rays. *Nat. Phys.*, **2014**, *11*, 69-74.
- [27] Ou-Yang, J.-K.; Saleh, N.; Fernandez Garcia, G.; Norel, L.; Pointillart, F.; Guizouarn, T.; Cador, O.; Totti, F.; Ouahab, L.; Crassous, J.; Le Guennic, B. Improved Slow Magnetic Relaxation in Optically Pure Helicene-Based Dy^{III} Single Molecule Magnet. *submitted*.

- [28] Wang, Y.; Li, X. L.; Wang, T. W.; Song, Y.; You, X. Z. Slow Relaxation Processes and Single-Ion Magnetic Behaviors in Dysprosium-Containing Complexes. *Inorg. Chem.* **2010**, *49*, 969-976.
- [29] Li, D.-P.; Wang, T.-W.; Li, C.-H.; Liu, D.-S.; Li, Y.-Z.; You, X.-Z. Single-ion magnets based on mononuclear lanthanide complexes with chiral Schiff base ligands [Ln(FTA)3L] (Ln = Sm, Eu, Gd, Tb and Dy). *Chem. Commun.* **2010**, *46*, 2929-2931.
- [30] Norel, L.; Bernot, K.; Feng, M.; Roisnel, T.; Caneschi, A.; Sessoli, R.; Rigaut, S. A carbon-rich ruthenium decorated dysprosium single molecule magnet. *Chem. Commun.* **2012**, *48*, 3948-3950.
- [31] Bosson, J.; Gouin, J.; Lacour, J. Cationic triangulenes and helicenes : synthesis, chemical stability, optical properties and extended applications of these unusual dyes. *Chem. Soc. Rev.* **2014**, *43*, 2824–2840.
- [32] Saleh, N.; Shen, C.; Crassous, J. Helicene-based transition metal complexes: synthesis, properties and applications. *Chem. Sci.* **2014**, *5*, 3680–3694.
- [33] Storch, J.; Zadny, J.; Strasak, T.; Kubala, M.; Syroka, J.; Dusek, M.; Cirkva, V.; Matejka, P.; Krbal, M.; Vacek, J. Synthesis and Characterization of a Helicene-Based Imidazolium Salt and its Application in Organic Molecular Electronics. *Chem. Eur. J.* **2014**, *21*, 2343-2347.
- [34] Mendola, D.; Saleh, N.; Hellou, N.; Vanthuyne, N.; Roussel, C.; Toupet, L.; Castiglione, F.; Melone, F.; Caronna, T.; Fontana, F.; Marti-Rujas, J.; Parisini, E.; Malpezzi, L.; Mele, A.; Crassous, J. Synthesis and Structural Properties of Aza[n]helicene Platinum Complex: Control of Cis and Trans Stereochemistry. *Inorg. Chem.* **2016**, *55*, 2009-2017.
- [35] Vacek, J.; Vacek Chocholousova, J.; Stara, I. G.; Sary, I.; Dubi, Y. Mechanical tuning of conductance and thermopower in helicene molecular junctions. *Nanoscale* **2015**, *7*, 8793-8802.
- [36] Jung, J., da Cunha, T. T., Le Guennic, B., Pointillart, F., Pereira, C. L. M., Luzon, J., Golhen, S., Cador, O., Maury, O. and Ouahab, L. Magnetic Studies of Redox-Active Tetrathiafulvalene-Based Complexes: Dysprosium vs. Ytterbium Analogues. *Eur. J. Inorg. Chem.*, **2014**: 3888–3894.
- [37] Cosquer, G.; Pointillart, F.; Golhen, S.; Cador, O.; Ouahab, L. Slow Magnetic Relaxation in Condensed versus Dispersed Dysprosium(III) Mononuclear Complexes. *Chem. Eur. J.* **2013**, *19*, 7895-7905.
- [38] da Cunha, T. T.; Jung, J.; Boulon, M.-E.; Campo, G.; Pointillart, F.; Pereira, C. L. M.; Le Guennic, B.; Cador, O.; Bernot, K.; Pineider, F.; Golhen, S.; Ouahab, L. Magnetic Poles Determinations and Robustness of Memory Effect upon Solubilization in a Dy^{III}-Based Single Ion Magnet. *J. Am. Chem. Soc.* **2013**, *135*, 16332-16335.
- [39] Saleh, N.; Moore, II, B.; Srebro, M.; Vanthuyne, N.; Toupet, L.; Williams, J. A. G.; Roussel, C.; Deol, K. K.; Muller, G.; Autschbach, J.; Crassous, J. Acid/Base-Triggered Switching of Circularly Polarized Luminescence and Electronic Circular Dichroism in Organic and Organometallic Helicenes. *Chem. Eur. J.* **2015**, *21*, 1673-1681.
- [40] Llunell, M.; Casanova, D.; Cirera, J.; Bofill, J. M.; Alemany, P.; Alvarez, S. S. SHAPE (version 2.1), Barcelona, 2013.
- [41] Kahn, O. *Molecular Magnetism*; VCH: Weinheim, **1993**.
- [42] Dekker, C.; Arts, A. F. M.; Wijn, H.W.; van Duyneveldt, A. J.; Mydosh, J. A. Activated dynamics in a two-dimensional Ising spin glass: Rb₂Cu_{1-x}Co_xF₄. *Phys. Rev. B* **1989**, *40*, 11243.
- [43] Cole, K. S.; Cole, R. H. Dispersion and Absorption in Dielectrics I. Alternating Current Characteristics. *J. Chem. Phys.* **1941**, *9*, 341.
- [44] Chibotaru, L. F.; Ungur, L. Ab initio calculation of anisotropic magnetic properties of complexes. I. Unique definition of pseudospin Hamiltonians and their derivation. *J. Chem. Phys.* **2012**, *137*, 064112–064122.

- [45] Chibotaru, L. F.; Ungur, L.; Soncini, A. The Origin of Nonmagnetic Kramers Doublets in the Ground State of Dysprosium Triangles: Evidence for a Toroidal Magnetic Moment *Angew. Chem., Int. Ed.* **2008**, *47*, 4126–4129.
- [46] Lunghi, A.; Totti, F. The role of Anisotropic Exchange in Single Molecule Magnets : A CASSCF/NEVPT2 Study of the Fe₄ SMM Building Block [Fe₂(OCH₃)₂(dbm)₄] Dimer. *Inorganics*, **2016**, *4*, 28–38.
- [47] Tesi, L.; Lunghi, A.; Atzori, M.; Lucaccini, E.; Sorace, L.; Totti, F.; Sessoli, R. Giant spin-phonon bottleneck effects in evaporable vanadyl-based molecules with long spin coherence. *Dalton Trans.* **2016**, *45*, 16635–16643.
- [48] Zadrozny, J. M.; Long, J. R. Slow Magnetic Relaxation at Zero Field in the tetrahedral Complex [Co(SPh)₄]²⁻. *J. Am. Chem. Soc.* **2011**, *133*, 20732–20734.
- [49] Freedman, D. E.; Harman, W. H.; Harris, T. D.; Long, G. H.; Chang, C. J.; Long, J. R. Slow Magnetic Relaxation in a High-Spin Iron(II) Complex. *J. Am. Chem. Soc.* **2010**, *132*, 1224–1225.
- [50] Vooshin, A. I.; Shavaleev, N. M.; Kazakov, V. P. Chemiluminescence of praseodymium (III), neodymium (III) and ytterbium (III) β-diketonates in solution excited from 1,2-dioxetane decomposition and singlet-singlet energy transfer from ketone to rare-earth β-diketonates. *J. Luminescence*, **2000**, *91*, 49–58.
- [51] Saleh, N.; Srebro, M.; Reynaldo, T.; Vanthuyne, N.; Toupet, L.; Chang, V. Y.; Muller, G.; Williams, J. A. G.; Roussel, C.; Autschbach, J.; Crassous, J. *enantio*-Enriched CPL-active helicene-bipyridine-rhenium complexes. *Chem. Commun.* **2015**, *51*, 3754–3757.
- [52] Aquilante, F.; De Vico, L.; Ferré, N.; Ghigo, G.; Malmqvist, P. A.; Neogady, P.; Bondo Pedersen, T.; Pitonak, M.; Reiher, M.; Roos, B. O.; Serrano-Andrés, L.; Urban, M.; Veryazov, V.; Lindh, R. MOLCAS 7: The Next Generation. *J. Comput. Chem.* **2010**, *31*, 224–247.
- [53] Roos, B. O.; Taylor, P. R.; Siegbahn, P. E. M. A complete active space SCF method (CASSCF) using a density matrix formulated super-CI approach. *Chem. Phys.* **1980**, *48*, 157–288.
- [54] Malmqvist, P. A.; Roos, B. O.; Schimmelpfennig, B. The restricted active space (RAS) state interaction approach with spin-orbit coupling. *Chem. Phys. Lett.* **2002**, *357*, 230–240.
- [55] Malmqvist, P. A.; Roos, B. O. The CASSCF state interaction method. *Chem. Phys. Lett.* **1989**, *155*, 189–194.
- [56] Aquilante, F.; Malmqvist, P.-A.; Pedersen, T.-B.; Ghosh, A.; Roos, B. O. Decomposition-Based Multiconfiguration Second-Order Perturbation Theory (CD-CASPT2): Application to the Spin-State Energetics of Co^{III}(diiminato)(NPh). *J. Chem. Theory Comput.* **2008**, *4*, 694–702.
- [57] Roos, B. O.; Lindh, R.; Malmqvist, P.-A.; Veryazov, V.; Widmark, P.-O. Main Group Atoms and Dimers Studied with a New Relativistic ANO Basis Set. *J. Phys. Chem. A* **2004**, *108*, 2851–2858.
- [58] Roos, B. O.; Lindh, R.; Malmqvist, P.-A.; Veryazov, V.; Widmark, P.-O. New Relativistic ANO Basis Sets for Transition Metal Atoms. *J. Phys. Chem. A* **2005**, *109*, 6576–6586.
- [59] Roos, B. O.; Lindh, R.; Malmqvist, P.-A.; Veryazov, V.; Widmark, P.-O.; Borin, A.-C. New relativistic Atomic Natural Orbital Basis Sets for lanthanide Atoms with Applications to the Ce Diatom and LuF₃. *J. Phys. Chem. A* **2008**, *112*, 11431–11435.
- [60] Frisch, M. J.; Trucks, G. W.; Schlegel, H. B.; Scuseria, G. E.; Robb, M. A.; Cheeseman, J. R.; Scalmani, G.; Barone, V.; Mennucci, B.; Petersson, G. A.; Nakatsuji, H.; Caricato, M.; Li, X.; Hratchian, H. P.; Izmaylov, A. F.; Bloino, J.; Zheng, G.; Sonnenberg, J. L.; Hada, M.; Ehara, M.; Toyota, K.; Fukuda, R.; Hasegawa, J.; Ishida, M.; Nakajima, T.; Honda, Y.; Kitao, O.; Nakai, H.; Vreven, T.; Montgomery, Jr. J. A.; Peralta, J. E.; Ogliaro, F.; Bearpark, M.; Heyd, J. J.; Brothers, E.; Kudin, K. N.; Staroverov, V. N.; Kobayashi, R.; Normand, J.; Raghavachari, K.; Rendell, A.; Burant, J. C.; Iyengar, S. S.; Tomasi, J.; Cossi, M.; Rega, N.; Millam, J. M.; Klene, M.; Knox, J. E.; Cross, J. B.; Bakken, V.; Adamo, C.; Jaramillo, J.; Gomperts, R.; Stratmann, R. E.; Yazyev, O.; Austin, A. J.; Cammi, R.; Pomelli, C.; Ochterski, J. W.; Martin, R. L.; Morokuma, K.; Zakrzewski,

- V. G.; Voth, G. A.; Salvador, P.; Dannenberg, J. J.; Dapprich, S.; Daniels, A. D.; Farkas, O.; Foresman, J. B.; Ortiz, J. V.; Cioslowski, J.; Fox, D. J. Gaussian 09, Revision A.02; Gaussian Inc.: Wallingford, CT, 2009.)
- [61] Perdew, J. P.; Burke, K.; Ernzerhof, M. Generalized Gradient Approximation Made Simple. *Phys. Rev. Lett.* **1996**, *77*, 3865–3868. (b) Adamo, C.; Barone, V. Toward reliable density functional methods without adjustable parameters: The PBE0 model. *J. Chem. Phys.* **1999**, *110*, 6158–6170.
- [62] Dolg, M.; Stoll, H.; Preuss, H. A combination of quasirelativistic pseudopotential and ligand field calculations for lanthanoid compounds. *Theor. Chim. Acta* **1993**, *85*, 441–450.
- [63] Weigend, F.; Ahlrichs, R. Balanced basis sets of split valence, triple zeta valence and quadruple zeta valence quality for H to Rn: Design and assessment of accuracy. *Phys. Chem. Chem. Phys.* **2005**, *7*, 3297–3305).